Spatiotemporal complexity of a ratio-dependent predator-prey system

Weiming Wang,[1,2,*] Quan-Xing Liu,[1,†] and Zhen Jin[1,‡]
[1]*Department of Mathematics, North University of China, Taiyuan, Shan'xi 030051, People's Republic of China*
[2]*School of Mathematics and Information Science, Wenzhou University, Wenzhou, Zhejiang 325035, People's Republic of China*
(Received 6 January 2007; published 21 May 2007)

In this paper, we investigate the emergence of a ratio-dependent predator-prey system with Michaelis-Menten–type functional response and reaction diffusion. We obtain the conditions of Hopf, Turing, and wave bifurcation in a spatial domain. Furthermore, we present a theoretical analysis of evolutionary processes that involves organisms distribution and their interaction of spatially distributed population with local diffusion. The results of numerical simulations reveal that the typical dynamics of population density variation is the formation of isolated groups, i.e., stripelike or spotted or coexistence of both. Our study shows that the spatially extended model has not only more complex dynamic patterns in the space, but also chaos and spiral waves. It may help us better understand the dynamics of an aquatic community in a real marine environment.

DOI: 10.1103/PhysRevE.75.051913 PACS number(s): 87.23.Cc, 89.75.Fb, 89.75.Kd, 47.54.−r

I. INTRODUCTION

Ecological systems are characterized by the interaction between species and their natural environment [1]. Such interaction may occur over a wide range of spatial and temporal scales [2,3]. The study of complex population dynamics is nearly as old as population ecology. In the 1920s, Lotka and Volterra independently developed a simple model of interacting species that still bears their joint names. This was a simple model, but the predator-prey version displayed neutrally stable cycles [4,5]. From then on, the dynamic relationship between predators and their prey has long been and will continue to be one of dominant themes in both ecology and mathematical ecology due to its universal existence and importance [6–8].

Predator-prey models follow two general principles: one is that population dynamics can be decomposed into birth and death processes; the other is the conservation of mass principle, stating that predators can grow only as a function of what they have eaten [9]. With these two principles we can write the canonical form of a predator-prey system as

$$\dot{N}(t) = Ng(N) - f(N,P)P - \mu_N(N)N,$$

$$\dot{P}(t) = \gamma f(N,P)P - \mu_P(P)P, \tag{1}$$

where t denotes time and $N(t), P(t)$ stand for prey and predator density, respectively, $g(N)$ is the per capita prey growth rate in the absence of predators, μ_N and μ_P are natural mortalities of prey and predator, respectively, and $f(N,P)$ is the functional response. And $\gamma f(N,P)$ is the per capita production of predators due to predation, which is often called the numerical response. Usually one considers consumption to be the major death cause for the prey. In this case $\mu_N(N)$ can be neglected and set to 0 (as long as the predator exists) [9].

In population dynamics, a functional response $f(N,P)$ of the predator to the prey density refers to the change in the density of prey attached per unit time per predator as the prey density changes [10]. In general, functional response can be classified as (i) prey dependent, when prey density alone determines the response, i.e., $f(N,P)=p(N)$; (ii) predator dependent, when both predator and prey populations affect the response. Particularly, when $f(N,P)=p(\frac{N}{P})$, we call model (1) strictly ratio dependent; and (iii) multispecies dependent, when species other than the focal predator and its prey species influence the functional response [11]. Differing from the prey-dependent predator-prey models, the ratio-dependent predator-prey systems have two principal predictions: (a) equilibrium abundance is positively correlated along a gradient of enrichment and (b) the "paradox of enrichment" either completely disappears or enrichment is linked to stability in a more complex way [12,13]. The ratio-dependent predator-prey model has been studied by several researchers recently and very rich dynamics have been observed [7,8,12,14,15].

On the other hand, we live in a spatial world, and spatial patterns are ubiquitous in nature, these patterns modify the temporal dynamics and stability properties of population densities at a range of spatial scales, their effects must be incorporated in temporal ecological models that do not represent space explicitly. And the spatial component of ecological interactions has been identified as an important factor in how ecological communities are shaped [1,2,8,16,17]. And pattern formation in nonlinear complex systems is one of the central problems of the natural, social, and technological sciences [16]. In particular, starting with the pioneering work of Segel and Jackson [18], spatial patterns and aggregated population distributions are common in nature and in a variety of spatiotemporal models with local ecological interactions [1,19]. Promulgated by the theoretical paper of Turing [20], the field of research on pattern formation modeled by reaction-diffusion systems, which provides a general theoretical framework for describing pattern formation in systems from many diverse disciplines including (but not limited to) biology [16,21–26], chemistry [27–32], physics [33–36], and so on, seems to be an increasingly interesting area, particularly during the last decade.

*Electronic address: weimingwang2003@163.com
†Electronic address: liuqx315@sina.com
‡Electronic address: jinzhn@263.net

In Ref. [2], Neuhauser surveyed some current work on spatial mathematical models in ecology. Much of this work consists of building spatial dimensions into existing classical models, such as the Lotka-Volterra model that describes competition between species. However, research on the spatial pattern of ratio-dependent predator-prey models seems to be rare.

II. STABILITY AND BIFURCATION ANALYSIS

In this paper, we mainly focus on the ratio-dependent predator-prey system with Michaelis-Menten-type (or Michaelis-Menten-Holling) functional response:

$$\frac{\partial N}{\partial t} = r\left(1 - \frac{N}{K}\right)N - \frac{\alpha N}{P + \alpha h N}P + D_1 \nabla^2 N,$$

$$\frac{\partial P}{\partial t} = \gamma \frac{\alpha N}{P + \alpha h N}P - \mu P + D_2 \nabla^2 P,$$

$$\forall (N,P) \in [0,\infty]^2 \setminus (0,0), \tag{2}$$

where N,P stand for prey and predator density, respectively. D_1, D_2 are their respective diffusion coefficients, $\nabla^2 = \frac{\partial}{\partial x^2} + \frac{\partial}{\partial y^2}$ is the usual Laplacian operator in two-dimensional space. All parameters are positive constants, r stands for maximal growth rate of the prey, γ conversion efficiency, μ predator death rate, K carrying capacity, α capture rate, and h handling time.

In the case of $P=0$ and $N>0$ we can define $f(N,0) := \frac{1}{h}$ [the limit of $f(x)$ for $x \to \infty$].

Let

$$\hat{N} = \frac{\alpha h N}{\gamma K}, \quad \hat{P} = \frac{\alpha h N}{\gamma^2 K}, \quad R = \frac{rh}{\gamma},$$

$$Q = \frac{h\mu}{\gamma}, \quad S = \frac{\alpha h}{\gamma}, \quad \hat{t} = \frac{\gamma t}{h}. \tag{3}$$

For simplicity we will not write the hat (^) in the rest of this paper. And in these new variables, from Eqs. (2) and (3), we arrive at the following equations containing dimensionless quantities:

$$\frac{\partial N}{\partial t} = R\left(1 - \frac{N}{S}\right)N - \frac{SN}{P + SN}P + D_1 \nabla^2 N,$$

$$\frac{\partial P}{\partial t} = \frac{SN}{P + SN}P - QP + D_2 \nabla^2 P. \tag{4}$$

More details about the choice of dimensionless variables in the system (2) as well as possible implications can be found in [14].

The dimensionless model [Eq. (4)] has five parameters: R, which controls the growth rate of prey; Q, which controls the death rate of the predator; S, which measures capturing rate; and $D_i (i=1,2)$, which defines the diffusion rates, respectively.

The first step in analyzing the model is to determine the behavior of the nonspatial model obtained by setting space derivatives equal to zero. The nonspatial model has at most three equilibria (stationary states), which correspond to spatially homogeneous equilibria of the full model [Eq. (4)], in the positive quadrant: (0, 0) (total extinct), $(S,0)$ (extinct of the predator), and a nontrivial stationary state (n^*, p^*) (coexistence of prey and predator), where

$$n^* = \frac{S[R + (Q-1)S]}{R},$$

$$p^* = \frac{S(1-Q)}{Q}n^* = \frac{S^2(R - S + QS)(1-Q)}{RQ}, \tag{5}$$

n^* is positive for all $S < \frac{R}{1-Q}$, which implies $Q<1$ and therefore ensures the positivity of p^* [14].

To perform a linear stability analysis, we linearize the dynamic system (4) around the spatially homogenous fixed point (5) for small space- and time-dependent fluctuations and expand them in Fourier space

$$N(\vec{x},t) \sim n^* e^{\lambda t} e^{i\vec{k}\cdot\vec{x}},$$

$$P(\vec{x},t) \sim p^* e^{\lambda t} e^{i\vec{k}\cdot\vec{x}}, \tag{6}$$

and obtain the characteristic equation

$$|A - k^2 D - \lambda I| = 0, \tag{7}$$

where

$$D = \begin{pmatrix} D_1 & 0 \\ 0 & D_2 \end{pmatrix}, \tag{8}$$

and A is given by

$$A = \begin{pmatrix} \partial_N f & \partial_P f \\ \partial_N g & \partial_P g \end{pmatrix}_{(n^*,p^*)} = \begin{pmatrix} f_N & f_P \\ g_N & g_P \end{pmatrix}, \tag{9}$$

where the elements are the partial derivatives of the reaction kinetics evaluated at the stationary state (n^*, p^*). Now Eq. (7) can be solved, yielding the so-called characteristic polynomial of the original problem [Eq. (4)]

$$\lambda^2 - \mathrm{tr}_k \lambda + \Delta_k = 0, \tag{10}$$

where

$$\mathrm{tr}_k = f_N + g_P - k^2(D_1 + D_2) = \mathrm{tr}_0 - k^2(D_1 + D_2), \tag{11}$$

$$\Delta_k = f_N g_P - f_P g_N - k^2(f_N D_2 + g_P D_1) + k^4 D_1 D_2$$
$$= \Delta_0 - k^2(f_N D_2 + g_P D_1) + k^4 D_1 D_2. \tag{12}$$

The roots of Eq. (10) yield the dispersion relation

$$\lambda_{1,2}(k) = \frac{1}{2}(\mathrm{tr}_k \pm \sqrt{\mathrm{tr}_k^2 - 4\Delta_k}). \tag{13}$$

The reaction-diffusion systems have led to the characterization of three basic types of symmetry-breaking bifurcations responsible for the emergence of spatiotemporal patterns. The space-independent Hopf bifurcation breaks the

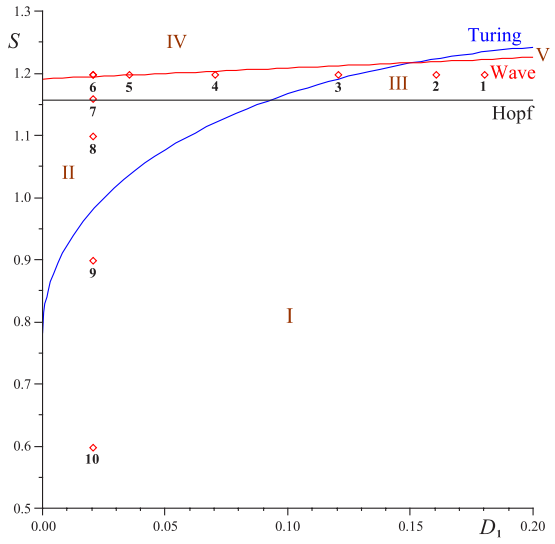

FIG. 1. (Color online) Bifurcation diagram for the system (2) with $R=0.5$, $Q=0.6$, $D_2=0.2$. Hopf bifurcation line: $S_H=\frac{37}{32}$; Turing bifurcation line: $S_T=-\frac{15}{32}D_1+\frac{375}{64}\sqrt{-\frac{12}{125}D_1{}^2+\frac{8}{125}D_1+\frac{25}{32}}$ with $k_T^2=1.29615$; wave bifurcation line: $S_W=(\frac{25}{16}D_1+\frac{5}{16})k_W^2+\frac{37}{32}$ with $k_W=0.334$. Turing-Hopf bifurcation point: (0.09248, 1.15625). Turing-wave bifurcation point: (0.15101, 1.21707). The numbers 1,2,3,4,5,6, and the points in line $S=1.2$ are the different selections of D_1, which correspond to the curves marked 1,2,3,4,5,6 in Fig. 2. And the numbers 10,9,8,7,6, and the points in line $D_1=0.02$ are the different selections of S, corresponding to Figs. 3–7.

temporal symmetry of a system and gives rise to oscillations that are uniform in space and periodic in time. The (stationary) Turing bifurcation breaks spatial symmetry, leading to the formation of patterns that are stationary in time and oscillatory in space. The wave (oscillatory Turing or finite-wavelength Hopf) bifurcation breaks both spatial and temporal symmetry, generating patterns that are oscillatory in space and time [29].

The Hopf bifurcation occurs when

$$\mathrm{Im}(\lambda(k)) \neq 0, \quad \mathrm{Re}(\lambda(k)) = 0 \quad \text{at } k = 0. \tag{14}$$

Then we can obtain the critical value of Hopf bifurcation parameter S equals

$$S_H = \frac{R + Q - Q^2}{1 - Q^2}. \tag{15}$$

At the Hopf bifurcation threshold, the temporal symmetry of the system is broken and gives rise to uniform oscillations in space and periodic oscillations in time with the frequency

$$\omega_H = \mathrm{Im}(\lambda(k)) = \sqrt{\Delta_0} = \sqrt{Q(Q-1)(R-S+QS)},$$

and the corresponding wavelength is

$$\lambda_H = \frac{2\pi}{\omega_H} = \frac{2\pi}{\sqrt{Q(Q-1)(R-S+QS)}}. \tag{16}$$

The Turing bifurcation occurs when

$$\mathrm{Im}(\lambda(k)) = 0, \quad \mathrm{Re}(\lambda(k)) = 0 \quad \text{at } k = k_T \neq 0. \tag{17}$$

The critical value of bifurcation parameter S equals

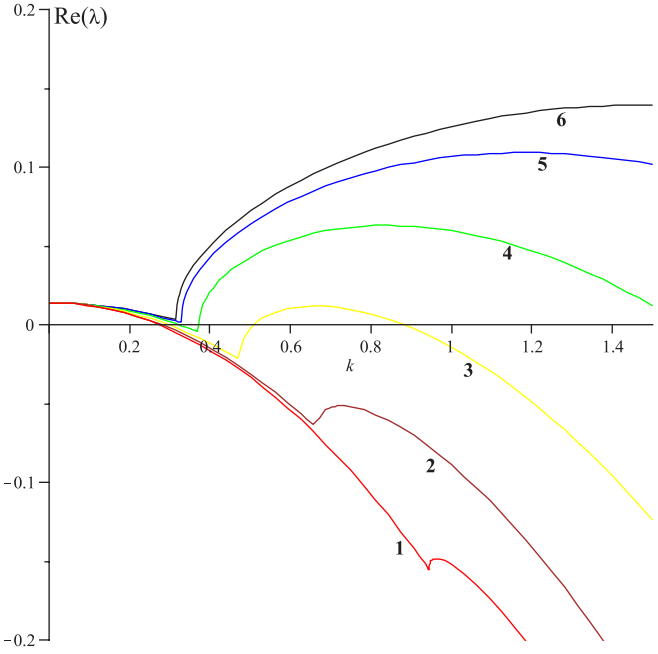

FIG. 2. (Color online) Dispersion relations showing unstable Hopf mode, transition of Turing and wave modes from stable to unstable for the system (2), e.g., as D_1 decreased. Parameters: $S=1.2$, $R=0.5$, $Q=0.6$, $D_2=0.2$, and (1) $D_1=0.18$; (2) $D_1=0.16$; (3) $D_1=0.12$; (4) $D_1=0.07$; (5) $D_1=0.035$; (6) $D_1=0.02$.

$$S_T = \frac{D_1 D_2 k_T^4 + [D_2 R + D_1 Q(1-Q)]k_T^2 + RQ(1-Q)}{Q^3 - (k_T^2 D_2 + 2)Q^2 + Q + k_T^2 D_2}, \tag{18}$$

where

$$k_T^2 = \sqrt{\frac{\Delta_0}{D_1 D_2}},$$

and at the Turing threshold, the spatial symmetry of the system is broken and the patterns are stationary in time and oscillatory in space with the wavelength

$$\lambda_T = \frac{2\pi}{k_T}. \tag{19}$$

The wave bifurcation occurs when

$$\mathrm{Im}(\lambda(k)) \neq 0, \quad \mathrm{Re}(\lambda(k)) = 0 \quad \text{at } k = k_w \neq 0. \tag{20}$$

The critical value of wave bifurcation parameter S equals

$$S_W = \frac{k_w^2(D_1 + D_2) + R + Q - Q^2}{1 - Q^2}, \tag{21}$$

where

$$k_w^2 = \frac{Q}{2D_2^2(Q+1)}[(D_1 - D_2)^2 Q^4 - 2(D_1^2 + D_2^2)Q^3 + (D_1^2 + D_2^2 + 6D_1 D_2 - 4D_2^2 R)Q^2 - 4D_1 D_2 Q + 4D_2^2 R]^{1/2}.$$

At the wave threshold, both spatial and temporal symmetries

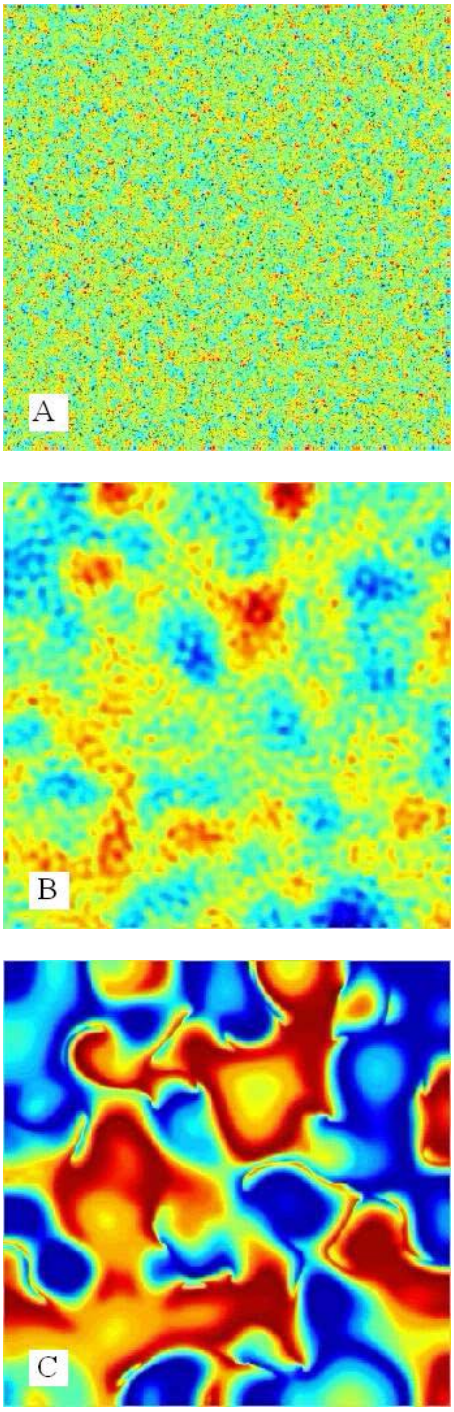

FIG. 3. (Color online) Snapshots of contour pictures of the time evolution of the prey at different instants with $S=0.6<S_T$. (A) 0 iteration; (B) 5000 iterations; (C) 45000 iterations [49].

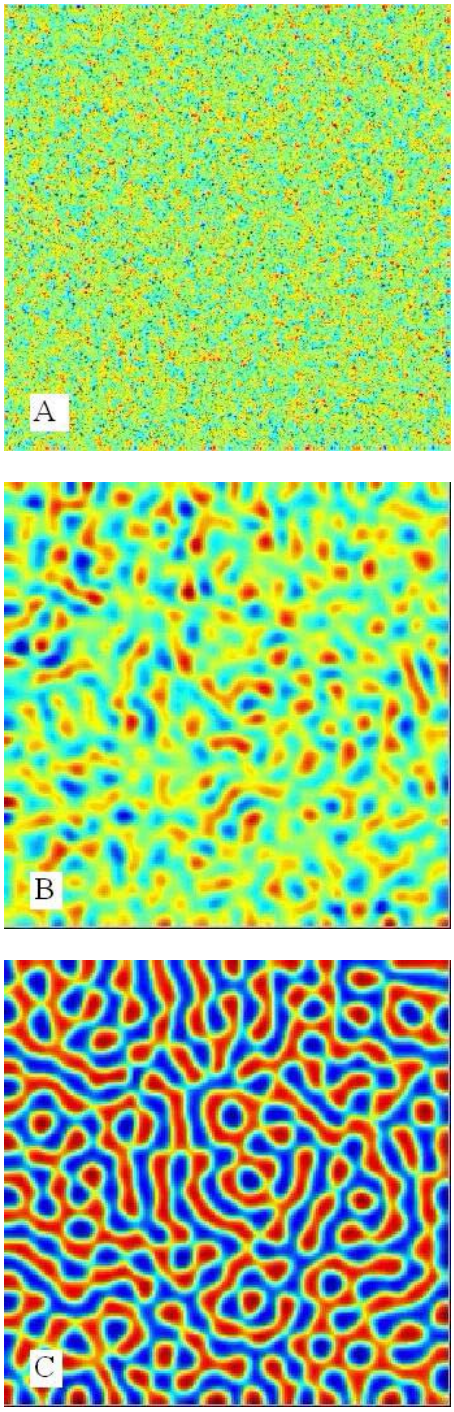

FIG. 4. (Color online) Snapshots of contour pictures of the time evolution of the prey at different instants with $S=0.9<S_T$. (A) 0 iteration; (B) 5000 iterations; (C) 45 000 iterations [49].

are broken and the patterns are oscillatory in space and time with the wavelength

$$\lambda_W = \frac{2\pi}{k_w}. \tag{22}$$

Linear stability analysis yields the bifurcation diagram with $R=0.5$, $Q=0.6$, $D_2=0.2$ shown in Fig. 1.

The Hopf bifurcation line, the wave bifurcation line, and the Turing bifurcation line intersect at two codimension-2 bifurcation points, the Turing-Hopf bifurcation point, and the Turing-wave bifurcation point. The bifurcation lines separate the parametric space into six distinct domains. In domain I, located below all three bifurcation lines, the steady state is the only stable solution of the system. Domain II is the region of pure Turing instabilities, and domain III is pure Hopf instabilities. In domain IV, both Hopf and Turing instabilities

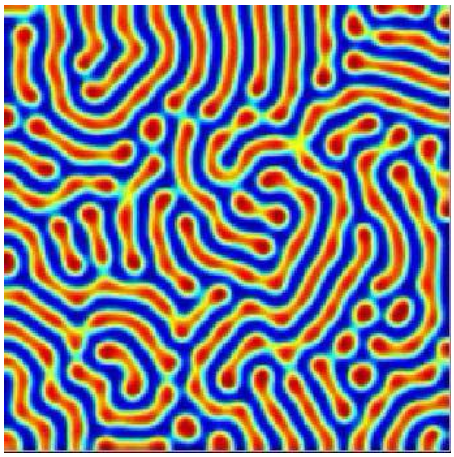

FIG. 5. (Color online) Snapshots of contour pictures of the time evolution of the prey at different instants with $S_T < S = 1.1 < S_H$ (45 000 iterations) [49].

occur, and in domain V, the wave and Hopf modes arise. When the parameters correspond to domain VI, which is located above all three bifurcation lines, all three instabilities occur. Figure 2 shows the dispersion relations of unstable Hopf mode, transition of Turing and wave modes from stable to unstable for the system (2). All three bifurcations are supercritical.

III. SPATIOTEMPORAL PATTERN ANALYSIS

In general, the predator-prey system with reaction diffusion, e.g., Eq. (4), describes the time evolution of the spatial distribution of species density. The nonuniform stationary states of the model, Eq. (4), that corresponds to spatial patterns cannot be found analytically. The analytical methods are not sufficient to fully understand the system, which is a reason for using computer simulations. That is to say, iterative computer simulations are required. If the model parameters are chosen appropriately the computer simulations will give rise to strikingly rich and surprising beautiful (such as stripelike, spotted, spiral, and spatial chaos) two-dimensional patterns.

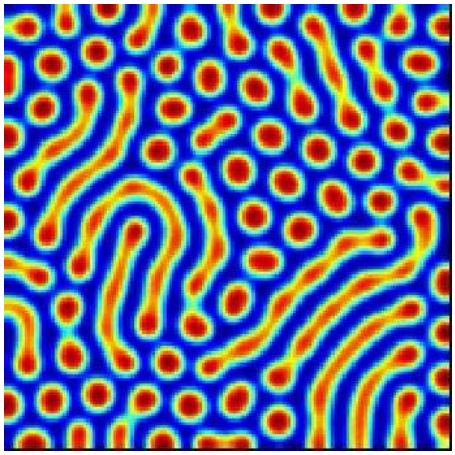

FIG. 6. (Color online) Coexistence of stationary spotted patterns and stripelike patterns of the prey for long time run with $S_H < S = 1.16 < S_W$ [49].

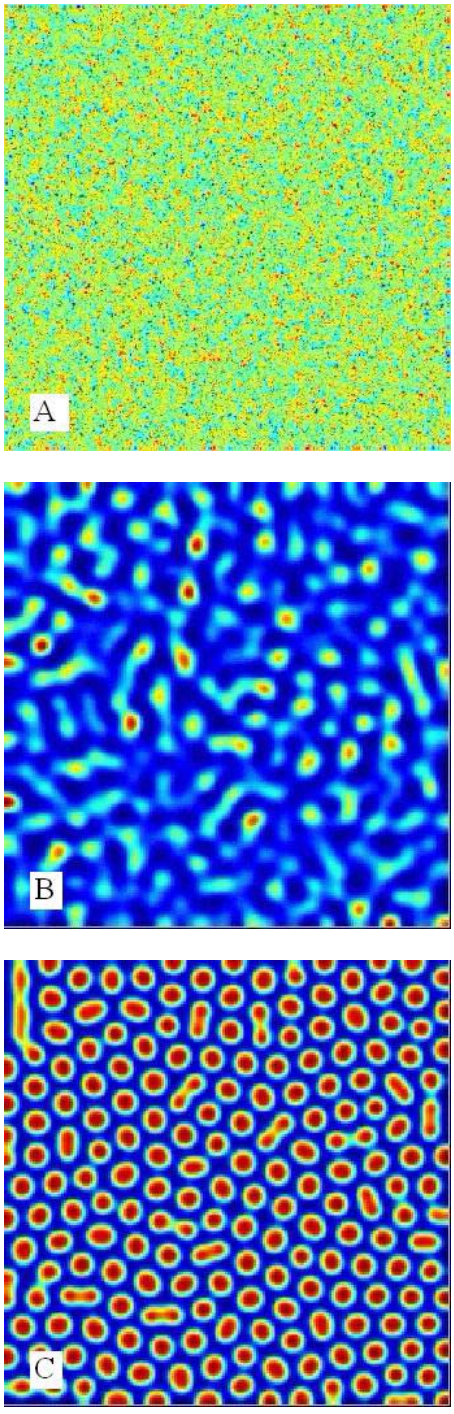

FIG. 7. (Color online) Snapshots of contour pictures of the time evolution of the prey at different instants with $S = 1.2 > S_W$. (A) 0 iteration; (B) 5000 iterations; (C) 45 000 iterations [49].

To solve differential equations, e.g., Eq. (4), by computers, one has to discretize the space and time of the problem, i.e., to transform it from an infinite-dimensional (continuous) to a finite-dimensional (discrete) form. In practice, the continuous problem defined by the reaction-diffusion system in two dimensions is solved in a discrete domain with $m \times n$ lattice sites. The spacing between the lattice points is defined

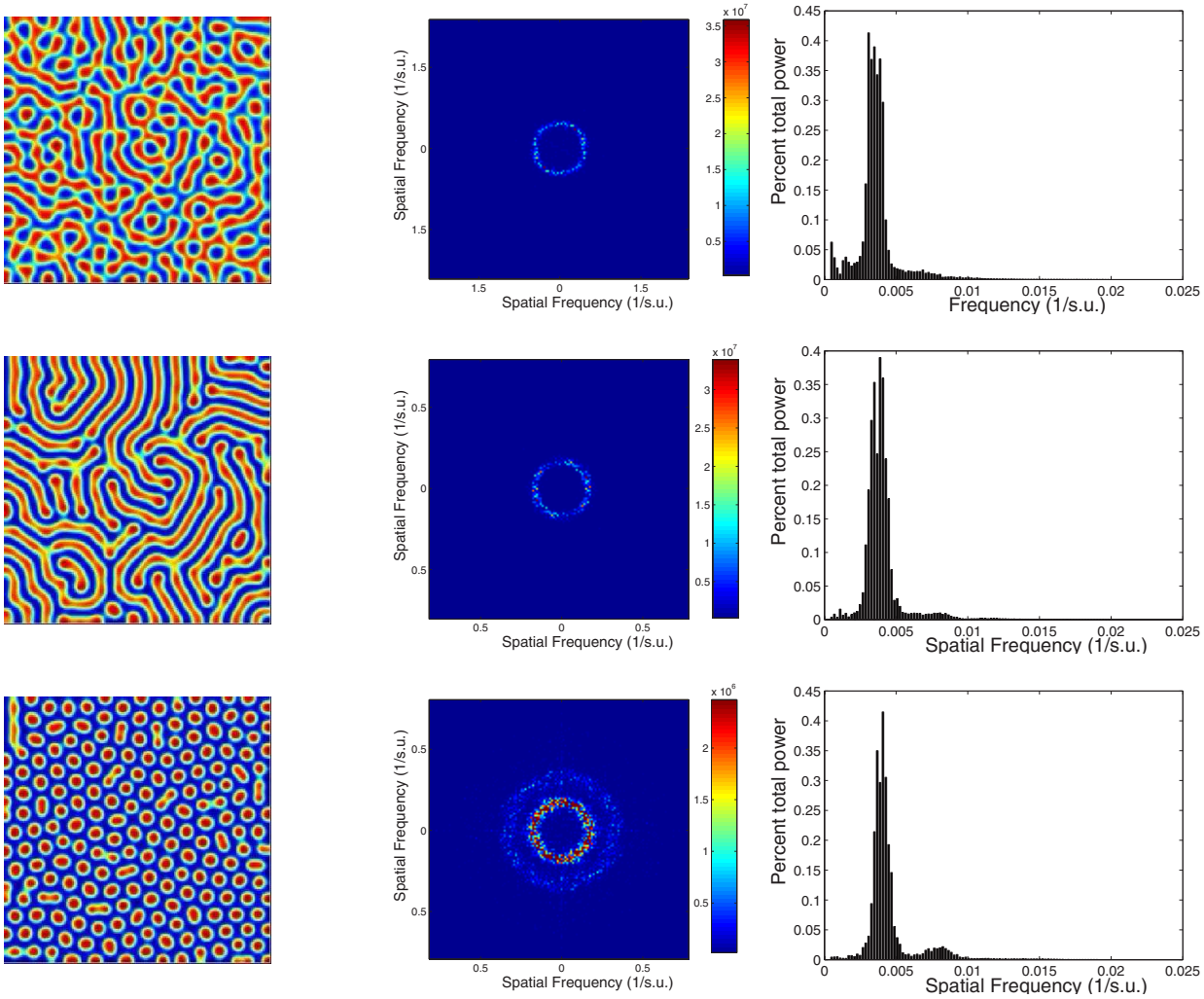

FIG. 8. (Color online) Patterns (left-hand column), spatial Fourier transformation (middle column), and radial average of the power spectrum (right-hand column). Top row $S=0.9$; Middle-row $S=1.1$; Bottom row $S=1.2$.

by the lattice constant Δh. In the discrete system the Laplacian describing diffusion is calculated using finite differences, i.e., the derivatives are approximated by differences over Δh. For $\Delta h \to 0$ the differences approach the derivatives. The time evolution is also discrete, i.e., the time goes in steps of Δt. The time evolution can be solved by using the so-called Euler method, which means approximating the value of the concentration at the next time step based on the change rate of the concentration at the previous time step [37].

In this section, we have performed extensive numerical simulations of the spatially extended model (4) in two-dimensional space, and the qualitative results are also shown. All our numerical simulations employ the periodic Neumann (zero-flux) boundary conditions with a system size of 200 $\times 200$ space units and $R=0.5$, $Q=0.6$, $D_1=0.02$, $D_2=0.2$. The spatiotemporal dynamics of a diffusion-reaction system depends on the choice of initial conditions, which some authors have considered in connection with the problem of biological invasion in a few papers [16,38–40], where the initial conditions are naturally described by some specific functions and the dynamics of the community mainly consists of a variety of diffusive populational fronts. In general, there are two initial conditions used for analysis of the spatial extended systems. One is random spatial distribution of the species, which seems to be more general from the biological point of view [cf. Figs. 3(a), 4(a), and 7(a)]. The other is a special choice, i.e., taking the species community in a horizontal layer as decreasing gradually and the vertical distribution of species homogeneity [cf. Fig. 9(a)]. In this section we choose the former, and the latter in Sec. IV. The equations (4) are solved numerically in two-dimensional space using a finite difference approximation for the spatial derivatives and an explicit Euler method for the time integration with a time stepsize of $\Delta t=0.01$ and space stepsize $\Delta h=0.25$.

From the analysis of Sec. II and phase-transition bifurcation diagram (cf. Fig. 1), the results of computer simulations show that the type of the system dynamics is determined by the values of S and D_1. We run the simulations until they reach a stationary state or until they show a behavior that does not seem to change its characteristics anymore. For different sets of parameters, the features of the spatial patterns become essentially different if S exceeds the critical value S_H, S_T, and S_W, respectively, which depend on D_1.

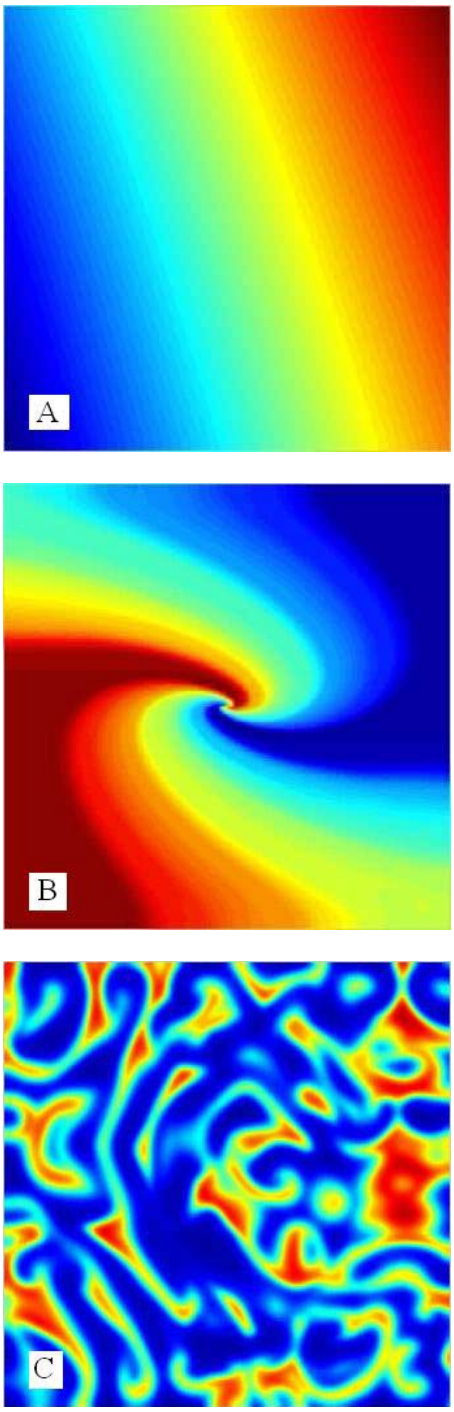

FIG. 9. (Color online) Snapshots of contour pictures of the time evolution of the prey at different instants with the special initial condition and $S=0.6<S_T$. (A) 0 iteration; (B) 1000 iterations; (C) 45 000 iterations [49].

Figure 3 shows the evolution of the spatial pattern of prey at 0, 5000, and 45000 iterations, with small random perturbation of the stationary solution n^* and p^* of the spatially homogeneous systems when S is less than the Turing bifurcation threshold S_T. In this case, one can see that for the system (4), the random initial distribution leads to the formation of a strongly irregular transient pattern in the domain. After the irregular pattern forms [cf. Fig. 3(b)], it grows slightly and "jumps" alternately for a certain time, and finally the chaos spiral patterns prevail over the whole domain, and the dynamics of the system does not undergo any further changes [cf. Fig. 3(c) and Ref. [49]].

Figures 4 and 5 show spontaneous formation of short stripelike and spotted spatial patterns emerge and coexist stably when the bifurcation parameter $S<S_T$ (Fig. 4) and $S_T<S<S_H$ (Fig. 5). From the snapshots or movies, one can see that the stripelike spatial patterns arise from the random initial conditions. After the stripelike patterns form [cf. Fig. 4(b)] they grow steadily with time until they reach certain width armlength, and the spatial patterns become distinct. Finally, the stripelike spatial patterns prevail the whole domain [cf. Fig. 4(c) and Fig. 5]. Comparing Figs. 4(c) with Fig. 5, we find that the parameter S is closer to S_T, and the stripelike spatial patterns are more distinct. Here we omit the preimage of Fig. 5 as they are similar to the Figs. 4(a) and 4(b). The stationary patterns are essentially different from the previous case (cf. Fig. 3).

When $S_H<S=1.16<S_W$, we find that the spotted patterns and the stripelike patterns coexist in the spatially extended model (cf. Fig. 6).

Figure 7 shows snapshots of prey spatial pattern at 0, 5000, and 45 000 iterations for the parameter $S=1.2>S_W$. Although the dynamics of the system starts from the same initial condition as previous cases, there is an essential difference for the spatially extended model [Eq. (4)]. From Fig. 7, one can see that the regular spotted patterns prevail over the whole domain at last, and the dynamics of the system does not undergo any further changes (cf. Ref. [49]).

On the other hand, discrete Fourier transform is a basic mathematical tool used to decompose a signal or image into different periodic components. It has been widely used for the spatial patterns [41–43]. We have also performed numerical investigations into two-dimensional space by Fourier spectra. The numerical computation of the Fourier transform is done by the well-established two-dimensional fast Fourier transform (FFT2) algorithm [44]. Spatial Fourier transform of the stripelike and spotted patterns in Figs. 4(c), 5, and 7(c) are shown as Fig. 8. And digital images (cf., Figs. 3–9) are obtained by using MATLAB (Ver. 7.0).

From Fig. 8, we find that Fig. 4(c)) and Fig. 5 have the same spatial frequency in the length of the space unit and presence of one mode with different wavelengths. On the contrary, Fig. 7(c)) has two modes with different wavelengths. The spatial frequency and direction of any component in the power spectrum are given in the length and direction, respectively, of a vector from the origin to the point on the circle. The magnitude is depicted by a gray scale or color scale, but the units are dimensionless values related to the total darkness of the original images. In Fig. 8 (middle column), short wavelength, represented by a large circle, corresponds to Turing structures; longer wavelength, represented by a small white circle, corresponds to traveling and/or standing waves. This technique can be particularly appropriate for characterizing quasiordered arrays for Fig. 7(c)).

IV. DISCUSSION AND CONCLUSION

The numerical results correspond perfectly to our theoretical findings that there are a range of parameters in $S-D_1$

plane where the different spatial patterns emerge (cf. Fig. 1). Figure 1 and the results of simulations present that the chaos patterns will persist in the spatially extended model [Eq. (4)] when the parameters are in the domain I. The boundary of this domain can be computed numerically and is shown as the blue line "Turing" in Fig. 1. The stationary state of stripelike patterns exists when the parameters are in the domain II, where its boundary can also be computed numerically and is shown as the black line "Hopf" in Fig. 1. The periodic spotted patterns appear in domain VI, where the boundary can be computed numerically by the wave bifurcation and is shown as the red line by the label of the "wave" in Fig. 1. Moreover, there is transverse domain IV (cf. Fig. 1) in the system between the stripelike patterns and spotted patterns, where the spotted patterns and the stripelike patterns coexist (cf. Fig. 6).

Do the stationary patterns arise dependent on the initial conditions? We test the different initial conditions for the spatially extended system, but the final spatial patterns are the same in qualitative. In those figures we find that the spatial chaos patterns come from the destruction of the spirals, when we choose the special initial condition (cf. Fig. 9) in domain I. This phenomenon coheres with the results of the study in Refs. [16,45].

We have presented a theoretical analysis of evolutionary processes that involves organisms distribution and their interaction of spatially distributed population with local diffusion. Our analysis and numerical simulations reveal that the typical dynamics of population density variation is the formation of isolated groups (stripelike or spotted or coexistence of both). This process depends on several parameters, including S, D_1, and D_2. The field meaning of our results may be found in the dynamics of an aquatic community which is affected by the existence of relatively stable mesoscale inhomogeneity in the field of ecologically significant factors such as water temperature, salinity, and biogen concentration.

In Ref. [16], the authors explained the field meaning by using aquatic community in the ocean (cf. Fig. 9). They had demonstrated phytoplankton and zooplankton spatiotemporal chaos patterns that emerged as a result of the fish school plankton interplay. It is apparent that the phytoplankton density is lower in the regions where zooplankton density is higher, and vice versa. Many previous observers have reported such an inverse relationship [46]. From the theoretical study on the 3D patterns [47], it is possible that the 3D patterns can be reflected by the 2D patterns. So our 2D spatial patterns may indicate the vital role of phase transience regimes in the spatiotemporal organization of the phytoplankton and zooplankton in the aquatic ecosystems. Our study shows that the spatially extended model [Eq. (4)] has not only more complex dynamic patterns in the space, but also chaos patterns and spiral waves, so it may help us better understand the dynamics of an aquatic community in a real marine environment. It is also important to distinguish between "intrinsic" patterns, i.e., patterns arising due to trophic interaction such as those considered above, and "forced" patterns induced by the inhomogeneity of the environment. The physical nature of the environmental heterogeneity, and thus the value of the dispersion of varying quantities and typical times and lengths, can be essentially different in different cases. Neuhauser and Pacala [48] formulated the Lotka-Volterra model as a spatial model. They found the striking result that the coexistence of patterns is actually harder to obtain in the spatial model than in the nonspatial one. One reason can be traced to how local interaction between individual members of the species are represented in the model. In this study, our results show that the ratio-dependent predator-prey model [Eq. (4)] also represents rich spatial dynamics, such as chaos spiral patterns, stripelike patterns, spotted patterns, coexistence of both stripelike and spotted patterns, etc. It will be useful for studying the dynamic complexity of ecosystems or physical systems.

ACKNOWLEDGMENTS

This work was supported by the National Natural Science Foundation of China under Grant No. 10471040 and the Natural Science Foundation of Shan'xi Province Grant No. 2006011009.

[1] M. Baurmann, T. Gross, and U. Feudel, J. Theor. Biol. **245**, 220 (2007).
[2] C. Neuhauser, Not. Am. Math. Soc. **47**, 1304 (2001).
[3] S. A. Levin, B. Grenfell, A. Hastings, and A. S. Perelson, Science **275**, 334 (1997).
[4] R. M. May, Nature (London) **261**, 459 (1976).
[5] B. E. Kendall, *Encyclopedia of Life Sciences* (Nature Publishing Group, London, 2001), Vol. 13, Chap. Nonlinear dynamics and chaos, pp. 255–262.
[6] A. A. Berryman, Ecology **73**, 1530 (1992).
[7] Y. Kuang and E. Beretta, J. Math. Biol. **36**, 389 (1998).
[8] J. D. Murray, *Mathematical Biology II: Spatial Models and Biomedical Applications*, 3rd ed. Biomathematics Vol. 18 (Springer, New York, 2003).
[9] C. Jost, Ph.D. thesis, Institute National Agronomique, Paris-Grignon, 1998.
[10] S. Ruan and D. Xiao, SIAM J. Appl. Math. **61**, 1445 (2001).
[11] P. A. Abrams and L. R. Ginzburg, Trends Ecol. Evol. **15**, 337 (2000).
[12] R. Arditi and L. R. Ginzburg, J. Theor. Biol. **139**, 311 (1989).
[13] M. L. Rosenzweig, Science **171**, 385 (1971).
[14] C. Jost, O. Arino, and R. Arditi, Bull. Math. Biol. **61**, 19 (1999).
[15] D. M. Xiao and L. S. Jennings, SIAM J. Appl. Math. **65**, 737 (2005).
[16] A. B. Medvinsky, S. V. Petrovskii, I. A. Tikhonova, H. Malchow, and B.-L. Li, SIAM Rev. **44**, 311 (2002).
[17] Q.-X. Liu, Z. Jin, and M.-X. Liu, Phys. Rev. E **74**, 031110 (2006).
[18] L. A. Segel and J. L. Jackson, J. Theor. Biol. **37**, 545 (1972).

[19] M. Pascual, Proc. R. Soc. London, Ser. B **251**, 1 (1993).
[20] A. M. Turing, Philos. Trans. R. Soc. London, Ser. B **237**, 7 (1952).
[21] C. A. Klausmeier, Science **284**, 1826 (1999).
[22] R. T. Liu, S. S. Liaw, and P. K. Maini, Phys. Rev. E **74**, 011914 (2006).
[23] J. von Hardenberg, E. Meron, M. Shachak, and Y. Zarmi, Phys. Rev. Lett. **87**, 198101 (2001).
[24] O. Lejeune, M. Tlidi, and P. Couteron, Phys. Rev. E **66**, 010901(R) (2002).
[25] E. Sharon, M. Marder, and H. L. Swinney, Am. Sci. **92**, 254 (2004).
[26] M. Pascual, M. Roy, and A. Franc, Ecol. Lett. **5**, 412 (2002).
[27] Q. Ouyang and H. L. Swinney, Nature (London) **352**, 610 (1991).
[28] V. K. Vanag, L. Yang, M. Dolnik, A. M. Zhabotinsky, and I. R. Epstein, Nature (London) **406**, 389 (2000).
[29] L. Yang, M. Dolnik, A. M. Zhabotinsky, and I. R. Epstein, J. Chem. Phys. **117**, 7259 (2002).
[30] L. Yang, M. Dolnik, A. M. Zhabotinsky, and I. R. Epstein, Phys. Rev. Lett. **88**, 208303 (2002).
[31] L. Yang and I. R. Epstein, Phys. Rev. Lett. **90**, 178303 (2003).
[32] L. Yang and I. R. Epstein, Phys. Rev. E **69**, 026211 (2004).
[33] W. Just, M. Bose, S. Bose, H. Engel, and E. Schöll, Phys. Rev. E **64**, 026219 (2001).
[34] M. C. Cross and P. C. Hohenberg, Rev. Mod. Phys. **65**, 851 (1993).
[35] A. Yochelis, A. Hagberg, E. Meron, A. L. Lin, and H. L. Swinney, SIAM J. Appl. Dyn. Syst. **1**, 236 (2002).
[36] T. Leppänen, M. Karttunen, R. A. Barrio, and K. Kaski, Phys. Rev. E **70**, 066202 (2004).
[37] T. Leppänen, Ph.D thesis, Helsinki University of Technology, Finland, 2004.
[38] J. Sherratt, M. Lewis, and A. Fowler, Proc. Natl. Acad. Sci. U.S.A. **92**, 2524 (1995).
[39] N. Shigesada and K. Kawasaki, *Biological Invasions: Theory and Practice* (Oxford University Press, Oxford, 1997).
[40] S. V. Petrovskii and H. Malchow, Theor Popul. Biol. **59**, 157 (2001).
[41] R. O. Prum and R. H. Torres, Integr. Comp. Biol. **43**, 591 (2003).
[42] R. O. Prum, R. Torres, S. Williamson, and J. Dyck, Proc. R. Soc. London, Ser. B **1414**, 13 (1999).
[43] R. O. Prum and R. Torres, J. Exp. Biol. **206**, 2409 (2003).
[44] W. L. Briggs and V. E. Henson, *The DFT* (Society for Industrial and Applied Mathematics, Philadelphia, PA, 1995).
[45] W. S. C. Gurney, A. R. Veitch, I. Cruickshank, and G. McGeachin, Ecology **79**, 2516 (1998).
[46] M. Fasham, Oceanogr. Mar. Biol. **16**, 43 (1978).
[47] T. Leppänen, M. Karttunen, K. Kaski, and R. A. Barrio, Int. J. Mod. Phys. B **17**, 5541 (2003).
[48] C. Neuhauser and S. W. Pacala, Ann. Appl. Probab. **9**, 1226 (1999).
[49] See EPAPS Document No. E-PLEEE8-75-142704 for a movie presentation. For more information on EPAPS, see http://www.aip.org/pubservs/epaps.html.